
Cold compression of nuclei induced by antiprotons

I.N. Mishustin · A.B. Larionov

the date of receipt and acceptance should be inserted later

Abstract On the basis of a dynamical Relativistic Mean Field (RMF) model we study the response of a nucleus on the antiproton implanted in its interior. We solve the Vlasov equation for the \bar{p} -nuclear system and show assuming a moderately attractive \bar{p} optical potential that the compressed state is formed on a rather short time scale of about $4 \div 10$ fm/c. The evolution of the system after \bar{p} annihilation is simulated using the Giessen Boltzmann-Uehling-Uhlenbeck (GiBUU) transport model. Finally, several sensitive observables to the \bar{p} annihilation in a compressed nuclear configuration are proposed, e.g. the nucleon kinetic energy spectra and the total invariant mass distributions of produced mesons.

Keywords \bar{p} -doped nuclei · nuclear compression · RMF model · BUU model

1 Introduction

Creation of the compressed nuclear matter in laboratory is a hot topic in the heavy ion community for more than three decades. The main interest here is to extract the information about the Equation of State of nuclear matter at high densities relevant for neutron star interiors. A well established way to produce compressed nuclear matter is to collide heavy ions with high energy. However, in this case the produced system will be not only compressed, but also quite strongly excited thermally.

Recently several authors [1,2,3,4,5] discussed the possibility to compress the nuclear system without much thermal excitation by implanting in it a hadron (Λ , \bar{K} , \bar{p} , $\bar{\Lambda}$) which has an attractive nuclear potential. It is believed that the antibaryon potentials are strongly attractive. The G -parity transformed proton potential is extremely deep: $U_{\bar{p}} \simeq -700$ MeV, while the phenomenological antiproton optical potential is much smaller $U_{\bar{p}} \simeq -(100 \div 350)$ MeV [6,7,8]. The static RMF calculations [3,4] predict a strong nuclear compression effect by \bar{p} and $\bar{\Lambda}$ even in the case of realistic potentials.

I.N. Mishustin · A.B. Larionov
Frankfurt Institute for Advanced Studies, J.W. Goethe-Universität, D-60438 Frankfurt am Main, Germany, and Russian Research Center Kurchatov Institute, 123182 Moscow, Russia
E-mail: mishustin@fias.uni-frankfurt.de

For instance, the central nucleon density of the ^{16}O core in the ground state $\bar{p} \otimes ^{16}\text{O}$ system is $(2 \div 4)\rho_0$, where $\rho_0 = 0.148 \text{ fm}^{-3}$ is the normal nuclear matter density.

A natural question which arises here is whether the early annihilation of an antibaryon will kill the effect of compression? A simple estimate of the stopped \bar{p} life time in nuclear matter at the normal density using vacuum annihilation cross section gives $\tau \simeq 2 \text{ fm}/c$. The phase space volume available in the baryon-antibaryon annihilation could be, however, essentially reduced due to smaller effective masses of the annihilating pair in nuclear matter. This effect can delay the annihilation up to $\sim 20 \text{ fm}/c$ [4].

In this talk we will present our results of dynamical simulations of \bar{p} -nuclear systems to demonstrate the compression dynamics and also to propose observable signals of possible \bar{p} annihilation in a compressed nuclear environment. Sect. 2 contains the short description of a model. The numerical results are collected in Sect.3, while the conclusions are given in Sect. 4.

2 The model

Here we give only a very brief review of our dynamical model. The detailed description of the GiBUU model applied in calculations and of its RMF extension can be found in refs. [5,9] and in refs. therein.

In calculations we use the RMF Lagrangian of Ref. [4], which includes the nucleon and antinucleon fields interacting with the isoscalar-scalar σ -meson field and with the isoscalar-vector ω -meson field. The NL3 set of parameters was used. This set provides a good description of nuclear matter and ground states of finite nuclei.

The antinucleon couplings with σ - and ω -fields were obtained by rescaling the nucleon coupling constants as $g_{\sigma\bar{N}} = \xi g_{\sigma N}$ and $g_{\omega\bar{N}} = -\xi g_{\omega N}$, where $0 < \xi \leq 1$ is a scaling factor. Exact G -parity transformed antinucleon scalar and vector fields are obtained by the choice $\xi = 1$. The antinucleon potentials consistent with the phenomenological ones are represented here by choosing $\xi = 0.3$.

The dynamics of interacting nucleons and an antiproton was described within the transport GiBUU model dealing with a coupled set of semiclassical kinetic equations (see [5] and refs. therein). The test particle technique in a parallel ensemble mode has been used to solve these equations.

An antiproton was initialized according to the gaussian density distributions in coordinate and momentum space. The centroids of the gaussians were set to describe the particle at the center of a nucleus ($\mathbf{r} = 0$) at rest ($\mathbf{p} = 0$). After initialization the system was left to evolve according to the kinetic equations without collision terms until \bar{p} annihilation at some preselected time moment t_{ann} . At this time a sudden annihilation of the antiproton with the closest nucleon was simulated on the basis of the string model JETSET. Once the annihilation is simulated, further evolution of the system of nucleons and mesons has been followed by solving the full kinetic equations including the collision terms. In this way, we have taken into account, in-particular, important processes of pion rescattering and absorption: $\pi N \rightarrow \Delta \rightarrow \pi N$ or $\pi N \rightarrow \Delta$, $\Delta N \rightarrow NN$.

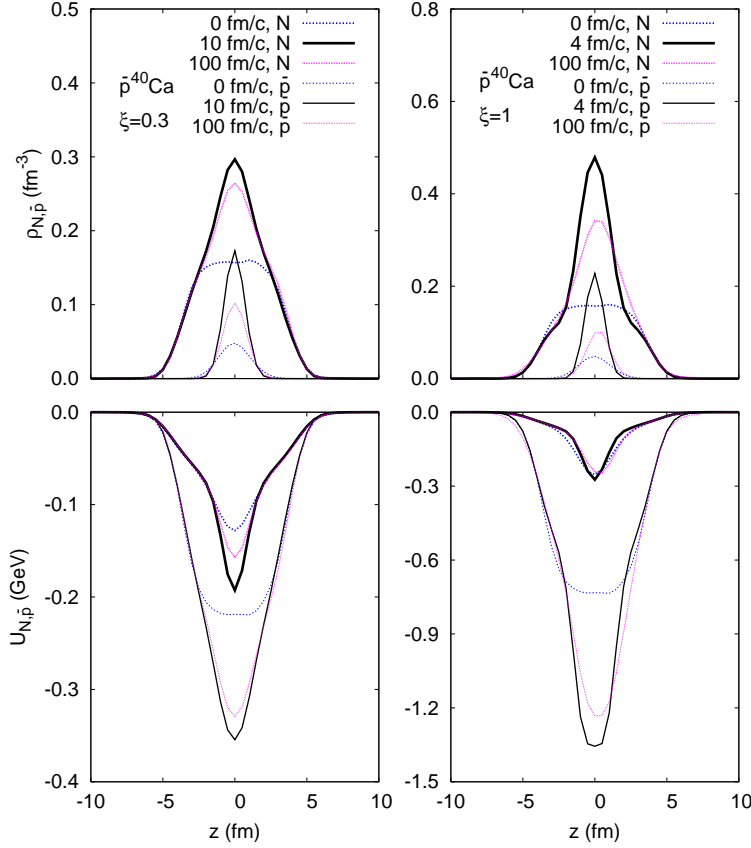


Fig. 1 Nucleon and antiproton densities (top panels) and potentials (bottom panels) vs coordinate z on the axis passing through the center of the $\bar{p}^{40}\text{Ca}$ system at selected times indicated in the figure. The calculations with the scaling factor $\xi = 0.3$ ($\xi = 1$) are shown in the left (right) panels.

3 Numerical results

First, we have studied the compression dynamics of a nucleus under the influence of an antiproton implanted in its center, completely neglecting the collision terms in kinetic equations, i.e. by taking into account the mean field only. The upper panels of Fig. 1 show the axial density distributions for nucleons and an antiproton at different times. In the lower panels of Fig. 1, the potentials defined as $U_j = g_{\omega j}\omega^0 + g_{\sigma j}\sigma$ ($j = N, \bar{p}$) are also shown. The nucleon density at the center grows quickly reaching its maximum already at $t = 10$ fm/c for the reduced \bar{p} -couplings and even faster at, $t = 4$ fm/c, for the G -parity-motivated couplings. The maximum nucleon density reached in this process is $\rho_N^{\max} \simeq 2\rho_0$ ($\rho_N^{\max} \simeq 3\rho_0$) for $\xi = 0.3$ ($\xi = 1$). The compression of the nuclear system leads also to the growth of the antiproton density at the center. The system stabilizes on the time scale of several tens fm/c.

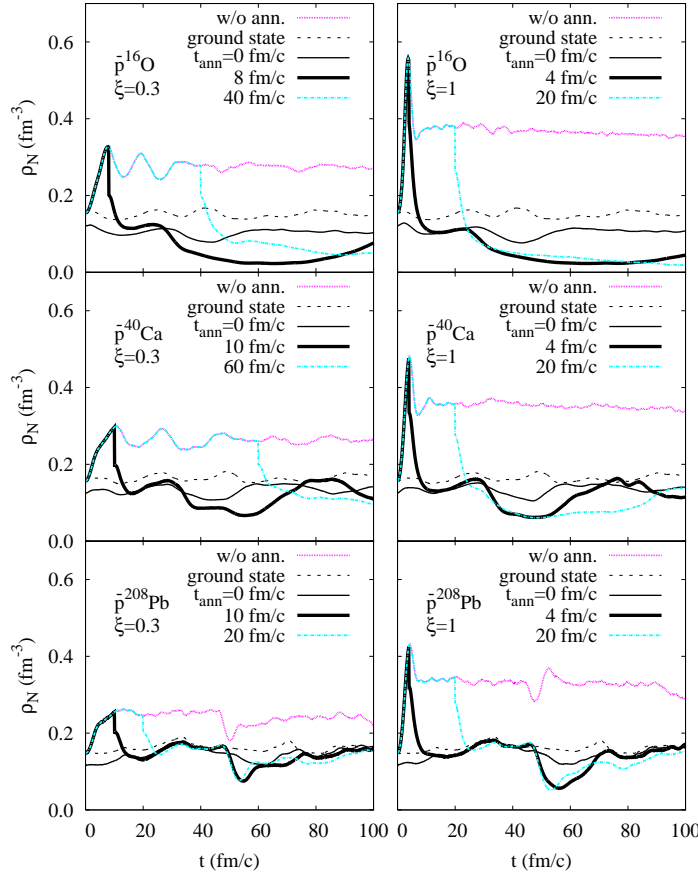


Fig. 2 Time evolution of the nucleon densities at the centers of the $\bar{p}^{16}\text{O}$, $\bar{p}^{40}\text{Ca}$ and $\bar{p}^{208}\text{Pb}$ systems for two values of the scaling factor $\xi = 0.3$ (left panels) and $\xi = 1$ (right panels). The dotted line shows the calculation without \bar{p} annihilation. The thin solid, thick solid and dash-dotted lines show the results with annihilation simulated at various times t_{ann} indicated in the figure. The dashed lines show the central nucleon density for the corresponding ground state nucleus without an antiproton.

Compression process is better demonstrated in Fig. 2, where the central nucleon density evolution is presented for the three systems: $\bar{p}^{16}\text{O}$, $\bar{p}^{40}\text{Ca}$ and $\bar{p}^{208}\text{Pb}$. For all the systems a compressed state is reached within $t = 4 \div 10$ fm/c and exists up to $t = 100$ fm/c. At later times the stability is gradually lost due to the test particle escape beyond the computational grid.

To understand how compression can possibly influence observables, we have simulated the annihilation of an antiproton at different preselected times t_{ann} . The evolution of a central nucleon density for different t_{ann} is also shown in Fig. 2. If the annihilation takes place in a compressed state, the system expands and, after $30 \div 40$ fm/c, the central density drops below ρ_0 . For the light and medium systems, $\bar{p}^{16}\text{O}$ and $\bar{p}^{40}\text{Ca}$, the central nucleon density stays below $0.6\rho_0$ for about $30 \div 50$ fm/c, which is sufficient

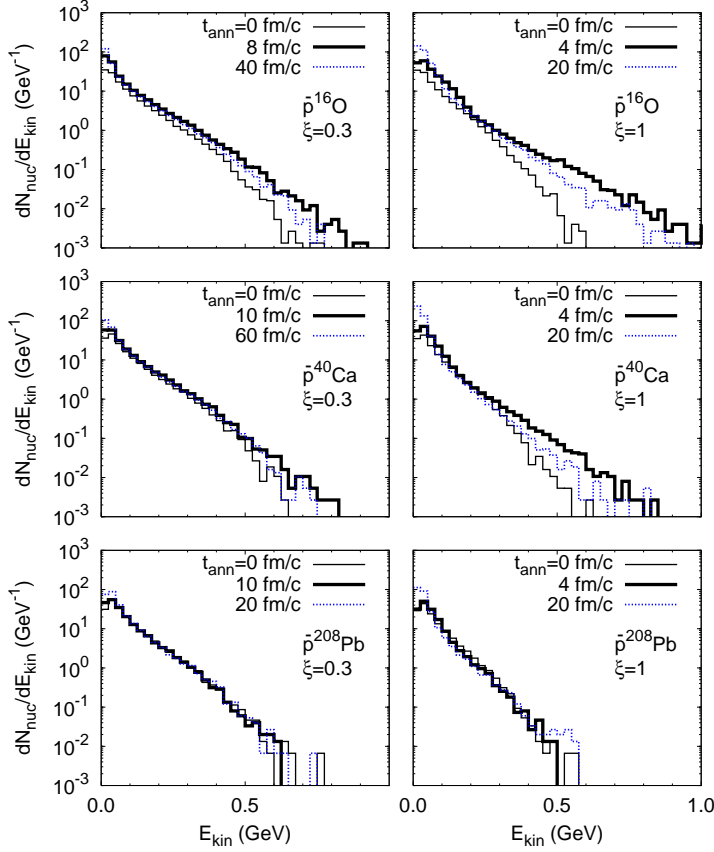


Fig. 3 Kinetic energy spectra of emitted nucleons in the c.m. frame for various $\bar{p}A$ systems and values of the parameter ξ as in Fig. 2. Different histograms correspond to different values of the annihilation time t_{ann} indicated in the key.

for the small density perturbations to grow according to the spinodal mechanism [10]. This process should eventually lead to the multiple fragment formation.

Fig. 3 shows the kinetic energy spectra of nucleons emitted from the system after \bar{p} -annihilation. They are mostly kicked-out by pion rescattering via intermediate $\Delta(1232)$ resonance: $\pi N \rightarrow \Delta \rightarrow \pi N$ [11]. In the case of annihilation in the compressed state, the nucleon spectrum acquires a high-energy tail with clearly stronger effect for lighter systems. This can be explained by the following mechanism: During the compression stage the nucleons in the central zone increase their kinetic energies due to falling down into the deep potential well created by the antiproton (see lower panels of Fig. 1). After \bar{p} -annihilation the potential well disappears suddenly, and the fast nucleons get released. This mechanism combined with additional kicks by pions leads to a visible enhancement of the energetic nucleon production.

In Fig. 4 we show the distribution of annihilation events in the total invariant mass M_{inv} of emitted mesons. In the absence of any in-medium effects, this distribution should be sharply peaked at $2m_N$. The final state interactions of mesons, i.e. rescat-

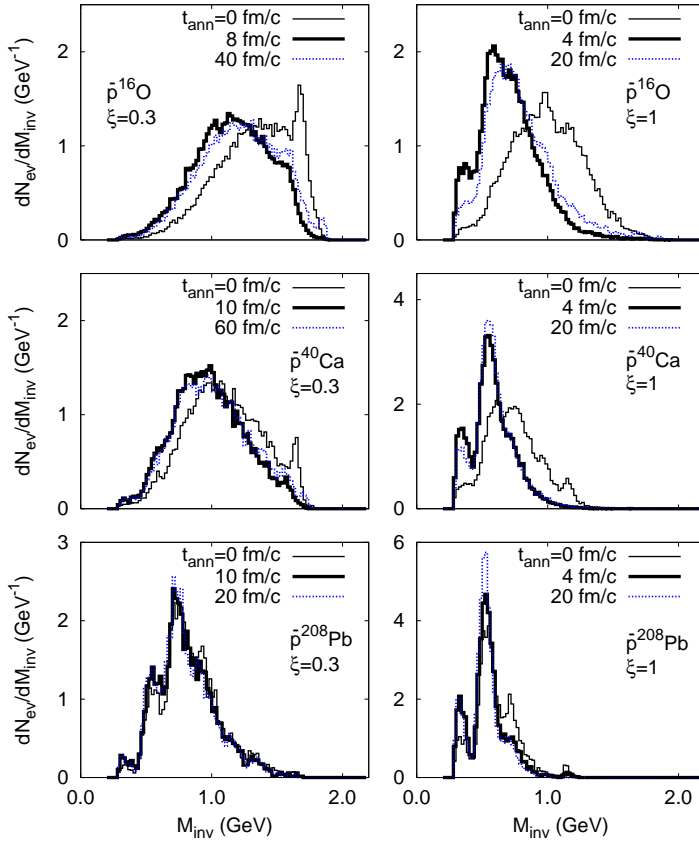


Fig. 4 Distributions of annihilation events in the total invariant mass of emitted mesons for various $\bar{p}A$ systems and values of the parameter ξ as in Fig. 2. Different histograms correspond to different values of the annihilation time t_{ann} indicated in the key.

tering and absorption on nucleons, lead to the strong spreading of the distribution toward smaller M_{inv} . Additionally, the mean-field effects reduce the invariant energy \sqrt{s} of annihilating \bar{p} -nucleon pair as $\sqrt{s} \simeq 2m_N + U_N + U_{\bar{p}} < 2m_N$. This further shifts the distribution to smaller M_{inv} . The effect is especially strong for annihilations in compressed configurations.

The above results have been obtained for the artificial case of an antiproton sitting at rest in the center of a nucleus. It is, certainly, more realistic to study the compression of the nucleus induced by moving \bar{p} . As an example, we have considered the central $\bar{p}^{12}\text{C}$ collision at $E_{\text{lab}} = 180$ MeV. In order to compute the mean field, we have performed simulations for 1000 parallel ensembles of test particles. The probability of \bar{p} -annihilation within the time interval Δt was calculated as $P_{\text{ann}} = 1 - \exp(-\Gamma_{\bar{p}}^{\text{ann}} \Delta t)$, where $\Gamma_{\bar{p}}^{\text{ann}}$ is the annihilation width and $\Delta t = 0.2$ fm/c is the time step of the simulation. In each run, the annihilation time for all parallel ensembles has been chosen randomly using P_{ann} . Further details of the model implementation for the \bar{p} -induced reactions on nuclei will be published elsewhere.

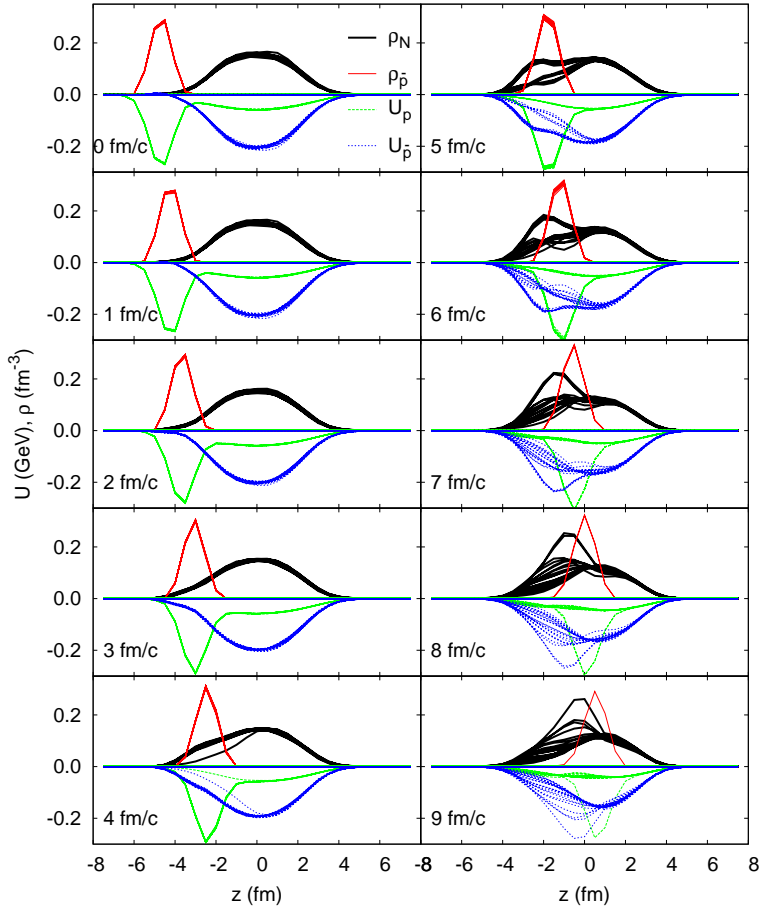


Fig. 5 Nucleon and antiproton density and potential profiles along collision axis at different time moments for the $\bar{p}(180 \text{ MeV})+^{12}\text{C}$ collision at the impact parameter $b = 0.5 \text{ fm}$. The mean field was computed with reduced \bar{p} couplings ($\xi = 0.3$).

In Fig. 5 we show the density distributions of nucleons and of the antiproton along the beam axis for 20 computed runs. One can see that in 19 runs the antiproton annihilation happened at the periphery of the nucleus. And only in a single run the antiproton has safely reached the central zone. In this run, the nucleon density has been increased up to $\simeq 2\rho_0$ by moving \bar{p} . This means that with $\sim 5\%$ probability one can expect the compression effect even in realistic central \bar{p} -nucleus collisions.

4 Conclusions

To summarise, we have performed the dynamical RMF calculations of the cold compression of nuclei by an antiproton implanted in their centers. The calculations in a pure mean field mode resulted in a fast increase of the central nucleon density up to $2 \div 3\rho_0$ within the time interval of $4 \div 10 \text{ fm/c}$. Without annihilation, the system stabilizes in a compressed state, which has been numerically traced until 100 fm/c . The

density profiles of compressed \bar{p} -nuclear systems are close to the ones obtained earlier by static RMF calculations [3,4].

Due to in-medium effects, the \bar{p} annihilation can be suppressed. In this case the time needed for a compression can be comparable with the life time of an antiproton with respect to the annihilation. Therefore, the compression can, indeed, manifest itself in some \bar{p} -nucleus collision events before the antiproton annihilation.

It has been demonstrated, that the events with nuclear compression have a probability of few percent even in $\bar{p}(180 \text{ MeV})+^{12}\text{C}$ central collisions. At higher energies, the fraction of the compression events is expected to be higher due to smaller \bar{p} -nucleon annihilation cross section.

In the present calculations we have used quite moderate values for the attractive real part of \bar{p} optical potential. Actual determination of $U_{\bar{p}}$ requires a very careful comparison with experimental data on elastic and inelastic scattering and absorption of antiprotons on nuclei. We propose to perform such measurements at the future FAIR facility in Darmstadt. In this respect we find very promising to use the event-by-event transverse momentum correlations proposed recently to determine the \bar{A} optical potential [12]. We believe that the same method can also be applied for the determination of the \bar{p} optical potential.

Acknowledgements We thank L.M. Satarov, W. Greiner, H. Stöcker, Th.J. Bürvenich and I.A. Pshenichnov for productive discussions. This work was supported in part by the DFG Grant 436 RUS 113/711/0-2 (Germany) and the Grant NS-3004.2008.2 (Russia).

References

1. Tanida, K. et al.: Measurement of the B(E2) of ${}^7_{\Lambda}\text{Li}$ and Shrinkage of the Hypernuclear Size. Phys. Rev. Lett. **86**, 1982-1985 (2001)
2. Akaishi, Y. and Yamazaki, T.: Nuclear \bar{K} bound states in light nuclei. Phys. Rev. C **65**, 044005 1-9 (2002)
3. Bürvenich, T., Mishustin, I.N., Satarov, L.M., Maruhn, J.A., Stöcker, H., and Greiner, W.: Enhanced binding and cold compression of nuclei due to admixture of antibaryons. Phys. Lett. B **542**, 261-267 (2002)
4. Mishustin, I.N., Satarov, L.M., Bürvenich, T.J., Stöcker, H., and Greiner, W.: Antibaryons bound in nuclei. Phys. Rev. C **71**, 035201 1-32 (2005)
5. Larionov, A.B., Mishustin, I.N., Satarov, L.M., and Greiner, W.: Dynamical simulation of bound antiproton-nuclear systems and observable signals of cold nuclear compression. Phys. Rev. C **78**, 014604 1-14 (2008)
6. Wong, C.-Y., Kerman, A.K., Satchler, G.R., MacKellar, A.D.: Ambiguity in antiproton-nucleus potentials from antiprotonic-atom data. Phys. Rev. C **29**, 574-580 (1984)
7. Teis, S., Cassing, W., Maruyama, T., and Mosel, U.: Analysis of subthreshold antiproton production in p-nucleus and nucleus-nucleus collisions in the relativistic Boltzmann-Uehling-Uhlenbeck approach. Phys. Rev. C **50**, 388-405 (1994)
8. Friedman, E., Gal, A., Mareš, J.: Antiproton-nucleus potentials from global fits to antiprotonic X-rays and radiochemical data. Nucl. Phys. A **761**, 283-295 (2005)
9. <http://theorie.physik.uni-giessen.de/GiBUU>
10. Chomaz, Ph., Colonna, M., and Randrup, J.: Nuclear spinodal fragmentation. Phys. Rep. **389**, 263-440 (2004)
11. Cahay, M., Cugnon, J., Jasselette, P. and Vandermeulen, J.: Antiproton annihilation inside nuclei. Phys. Lett. B **115**, 7-10 (1982)
12. Pochodzalla, J.: Exploring the potential of antihyperons in nuclei with antiprotons. arXiv:0807.3302v2 and contribution to these proceedings